

# ENHANCED LOSS PREDICTION FOR ADMISSION THROUGH CIRCUMFERENTIAL SLOTS IN AXIAL STEAM TURBINES

*D. Engelmann – A. Schramm – T. Polklas\* – M. A. Schwarz\* – R. Mailach*

Ruhr-Universität Bochum, Chair of Thermal Turbomachinery, 44780, Bochum, Germany,  
David.Engelmann@rub.de

\* MAN Diesel & Turbo SE, 46145, Oberhausen, Germany

## ABSTRACT

Steam turbines used in industrial applications usually contain branches for the admission and/or extraction of process steam at specific pressure levels. In most cases such branches are placed at the axial connections of two stage groups. Losses appearing at these junctions are caused by wall friction, mixing of several flow partitions and interaction with adjacent stage rows. In the current work a three stage steam turbine configuration, which includes a circumferential slot for steam admission, is examined. In order to estimate the pressure loss depending on additional inflow, similarity to combining flow in a pipe junction is used. In a parameterised numerical study several fluids and turbulence models are compared and validated with measurements. After that, gathered insights of the parameter study are applied to the steam turbine configuration, where common features as well as differences to the pipe junction are illustrated.

## NOMENCLATURE

A	-	area
AR	-	area ratio
FR	-	flow ratio $\dot{m}_{\text{Bleed}}/\dot{m}_{\text{AC,Out}}$
Ma	-	Mach number
$\dot{m}$	kg/s	mass flow
N	rpm	rotational speed
p	Pa	pressure
Re	-	Reynolds number
T	°C	temperature
V	m/s	velocity

### Greek Symbols

$\zeta$	-	pressure loss coefficient
$\Pi$	-	pressure ratio
$\tau_w$	N/m <sup>2</sup>	wall shear stress

### Subscripts

AC	axial connection
CS	cross sectional
fr	friction
In	inlet
Out	outlet
sec	secondary
Sf	surface
t	total

### Abbreviations

BSL	baseline
C	case
H	channel height
IAC	isolated axial connection
J	junction
R	fillet radius
RM	reattachment modification
S	stages
SST	shear stress transport
STC	steam turbine configuration

## INTRODUCTION

Modern steam turbines used in industrial applications, such as captive power plants for paper mills, mining, food production or the chemical industry, are often based on a modular and compact design. That means the control stage as well as various interchangeable high, intermediate and low pressure modules are combined together within a single turbine casing. Usually, several branches are included for the admission and/or extraction of process steam at specific pressure levels. These branches can be placed at the axial connections of two stage groups or within a single module. Due to variation in rotational speed, degree of admission and steam parameters, severe partial load conditions can occur and have to be taken into account to enable a high efficiency and a stable operational behaviour. Hence, it is important to estimate operational characteristics and loss mechanisms appearing at these junctions and connections already during the design process.

In literature several loss mechanisms are described for turbines with shrouded blades and the interaction with adjacent blade rows. Pfau et al. (2003) and Schlienger et al. (2003) investigated the shroud cavity flow of a two stage axial steam turbine. They focused on cavity vortices, their influence on subsequent rows and described alternative cavity outlet geometries to reduce the mixing losses. A 1.5 stage configuration of an axial low speed air turbine with shrouded blades was part of several investigations. Peters et al. (2000) and Anker and Mayer (2002) described the impact of tip clearance on the downstream flow field whereas Giboni et al. (2004) measured time resolved secondary flow fluctuations between adjacent stages. Denton (1993) provided several relations for losses caused by mixing of the re-entering shroud cavity flow with the main channel flow. Some more loss mechanisms are given by Wallis et al. (2000). They investigated turning device configurations to reduce shroud cavity losses in a four stage axial turbine and reported four loss types depending on labyrinth seals, counter rotating cavity walls, flow mixing at cavity outlet and following stages. Gier et al. (2003) adapted those loss definitions to a numerical prediction of a three stage low pressure turbine for jet engines and added another loss mechanism caused by steps in the flow path.

As stated above, loss mechanisms for shrouded blades and the interaction with downstream rows are described in detail. However, there exists a lack of information concerning losses caused by the deflection and mixing process of the admitted steam. Especially in 1D design tools only wall friction as a function of the axial length between two stage groups is estimated. Thus, the influence of turning, mixing and separation of mass flow partitions is often regarded insufficiently.

Engelmann et al. (2012) examined numerical predictions of a steam turbine configuration with focus on the axial connection between the high and intermediate pressure module containing a circumferential slot for steam admission (see Figure 1). As they illustrate, further losses can occur depending on the geometry of the junction and the amount of admitted steam. On the one hand the additional inflow mixes with flow partitions of the main channel and the shroud cavity outlet. On the other hand the inflow is turned from radial in axial flow direction, thereby remains near casing located, influences the incident flow to subsequent stages and changes the profile loading.

An approach to determine the pressure loss for the stage connection caused by the additional inflow is the use of analogy with combining flow in a pipe junction. Therefore, in the first part of the current work, a typical 90 degree T-junction, piece of copious experiments of Idelchik (1986) and Miller (1990), is used in a parameterised numerical study for combining flow of wide scope. A description of the simulation procedure realised in the programming language PERL with integration of the commercial mesh creator ICEM CFD and the numerical solver ANSYS CFX is considered first, followed by a specification of the used simulation parameters. Then the calculation of the secondary loss ensuing from total pressure loss and rate of friction is explained and compared with the experimental results. In the second part of this work gained insights from the T-junction computations are applied to the three stage configuration (STC) of Engelmann et al. (2012), where similarities and differences of the loss partitions in comparison to the parameter study are pointed out.

## STEAM TURBINE CONFIGURATION

Figure 1 illustrates the numerical region of the three-stage STC containing a circumferential slot at the axial connection of the first rotor row (last stage of high pressure group) and the second stator row (first stage of intermediate pressure group). Leakage steam coming up at the control stage and there used for axial thrust balancing is guided back to the main flow path through this slot. The flow ratio FR (slot flow related to outlet flow) amounts to 5.3 % at the design point and was varied in a range from 0% to 8%. Principal flow and geometric parameters applied to the STC are listed in Table 1. Further information about modelling, meshing, simulation setup and also explanations about the flow field within the axial gap are given in a prior publication of Engelmann et al. (2012).

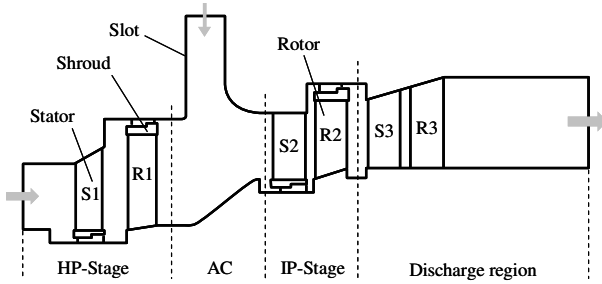


Figure 1: Model of investigated STC

Table 1: List of STC flow parameters

Rotational Speed $N$	15,400 RPM
Pressure Ratio $\Pi_{In-Out}$	2.51
Mach number $Ma_{AC, In}$	0.18
Reynolds number $Re_{AC, In}$	$6.38 \cdot 10^5$
Flow Ratio FR (design point)	5.3 %
Temperature $T_{AC, In}$	150 °C
Velocity $V_{AC, In}$	130 m/s
Area Ratio $AR_{AC}$	33 %
Fillet Ratio $R_{casing}/H_{AC, Out}$	0.48

## PARAMETER STUDY FOR COMBINING FLOW

A lot of numerical simulations have to be performed to depict and compare the characteristic loss curves given by Idelchik (1986) and Miller (1990). With the parameterised study it is possible to automate the simulation process and calculate the losses for a huge combination of mass flow and area ratios as well as for several turbulence models and fluids.

Idelchik and Miller investigated combining flow for pipe junctions with water as fluid. In contrast to this in the STC a circumferential slot exists and vapour is used. Despite geometric differences, both topologies feature radial inflow and 90 degree deflection related to the main flow path. Thus, a parameterised geometry is chosen which mirrors primary inflow and deflection behaviour and at the same time can automatically be built and meshed during the numerical study.

### Geometry and numerical grid

In order to automate the geometry creation process in ICFM-CFD with as few independent parameters as possible, the pipe junction system is modified and transformed into a translational periodic 2-dimensional T-junction system, whereas area ratios are preserved during the geometry transformation (see Figure 2, left). On the one hand this flat system better corresponds with the STC and its circumferential slot. On the other hand with such a rectangular model the geometry and also mesh creation routine is more convenient than with a complex 3D pipe system. Because Idelchik and Miller only mention area ratios and mass flow ratios, but no absolute pipe sizes, length values are taken from the STC to model the T-junction.

Major geometric parameters of the T-junction are given in the schematic drawing in the middle of Figure 2. There *distance a* is the hydraulic diameter of the main flow path and reference for all other length and area values. The diameter of the bleed represented by *width b* is calculated in dependency of the actual area ratio  $AR$  and *distance a*. All other geometry details such as vertices and curves are generated as a function of the two mentioned distances. According to Idelchik and Miller each flow section is as 70-times long as *distance a*. This supports a full developed velocity profile for inlet and bleed region. Furthermore, fluctuations and flow separations caused by deflection are able to decay before reaching the outlet of the numerical domain.

A block structured hexahedron mesh is used for the simulation with mesh refinements at the walls to resolve boundary layer effects (right side of Figure 2). In the same way the grid density is

successively increased starting from the domain boundaries to the junction region. Thus, the numerical region consists of in total 64,000 elements per 2D layer.

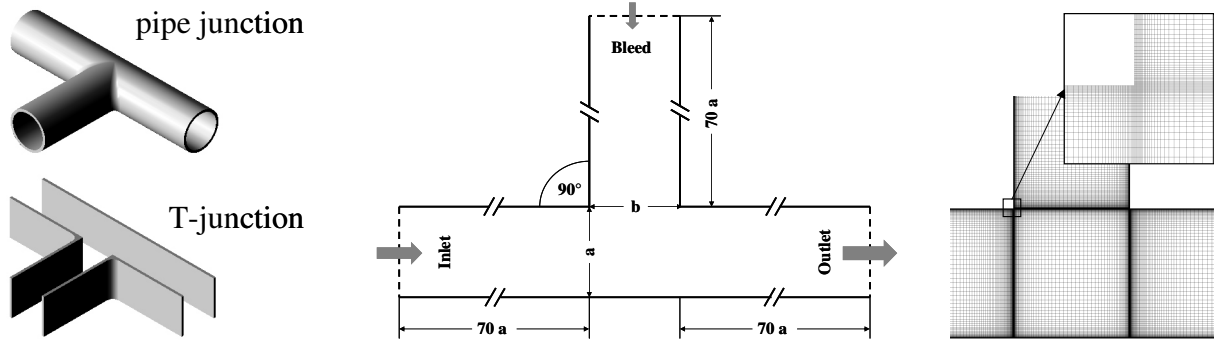


Figure 2: Geometric differences of pipe junction and T-junction (left); 2D T-junction geometry parameters (mid); mesh details (right)

### Numerical test cases

The flow field is computed with the commercial solver ANSYS-CFX. Overall 9 test cases are performed that fall into two main groups: fluids (C0 to C5) and  $k-\omega$  based turbulence models (C5 to C8). While Idelchik and Miller ran their measurements with water, superheated steam is applied to the STC. Strictly speaking, water vapour as single-phase real gas in accordance with the international properties steam table IAPWS-IF97 of Wagner et al. (2000) is used in combination with the SST-RM turbulence model. Therefore, within the first test case group thermodynamic parameters are gradually approached from water (C0) to STC data (C5) in order to point out whether there are differences in the loss results depending on the use of a specific fluid (compare Table 1 and 2). The second group contains several turbulence models in order to reveal variations compared to the SST-RM model. An overview of all performed test cases is given in Table 2.

Table 2: List of test cases used for parameter study

case	medium	T [°C]	$V_{in}$ [m/s]	$Re_{in}$	turbulence model	heat transfer
C0	water	25	5	$2.15 \cdot 10^5$	SST-RM	isothermal
C1	air, ideal gas	25	60	$2.09 \cdot 10^5$	SST-RM	isothermal
C2	air, ideal gas	150	80	$2.08 \cdot 10^5$	SST-RM	isothermal
C3	air, ideal gas	150	80	$2.09 \cdot 10^5$	SST-RM	total energy
C4	vapour, ideal gas	150	130	$4.06 \cdot 10^5$	SST-RM	total energy
C5	vapour, IF 97	150	130	$4.06 \cdot 10^5$	SST-RM	total energy
C6	vapour, IF 97	150	130	$4.06 \cdot 10^5$	SST	total energy
C7	vapour, IF 97	150	130	$4.06 \cdot 10^5$	BSL	total energy
C8	vapour, IF 97	150	130	$4.06 \cdot 10^5$	$k-\omega$	total energy

### Simulation procedure

A procedure written in the programming language PERL is used to realise the parameterised simulation study. Within the procedure it is possible to directly integrate, call up and mostly automate geometry creation, meshing and iteration process through so called replay- and session-scripts. Figure 3 illustrates the PERL procedure schematically. In general, it consists of an outer and an inner loop as well as sub-routines to control ICEM-CFD and ANSYS-CFX.

Fluid and turbulence model are set in the initial file. Then for a given set of parameters (initial file) the *width*  $b$  equivalent to the area ratio AR (Figure 2, left) is gradually reduced in the outer loop until the smallest width is reached. For a constant area ratio AR the inflow through the bleed starting from a zero-value is stepwise increased in the inner loop until the maximum inflow is reached. Parallel to this the inlet mass flow is decreased in the same way to keep a constant outlet mass flow. For both loops an increment of 10 % is used. Within the four sub-routines (ICEM, PRE, SOLVE, POST in Figure 3) several operations are executed. The corresponding programs are called. Initial- or layout-files are launched (grey boxes in Figure 3). Text-based replay-scripts are executed which are previously edited through variables containing e.g. geometry coordinates or directory names. At the end of a sub-routine task either result files are written which are used in the continuing procedure or CSV data are exported for evaluation and display in charts. In total about 600 calculations are performed including predictions for several turbulence models, fluids, flow parameters as well as various area and flow ratios.

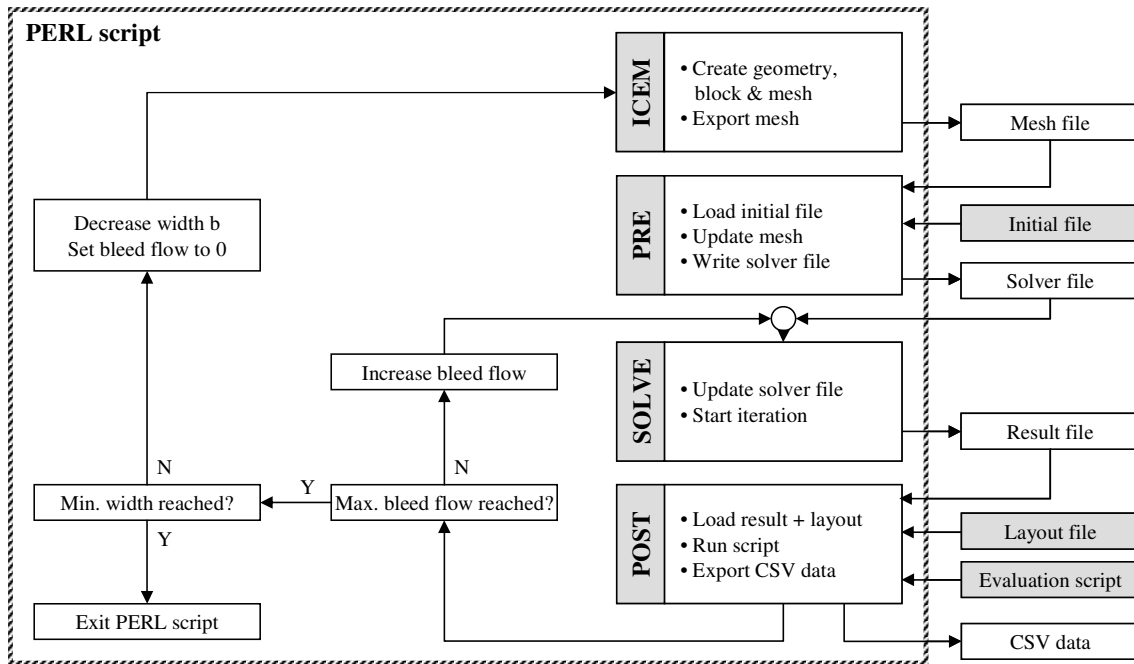


Figure 3: Scheme of T-junction parameter study realised in PERL

### Loss description for combining flow

Total pressure loss contains on the one side friction loss appearing at the walls and on the other side secondary loss induced by flow separation, vortex shedding, flow deflection and so forth. Idelchik and Miller describe the deflection loss in terms of total pressure loss coefficient but without pipe friction loss. Thus, to compare the secondary losses of the numerical predictions with the experimental data, several loss types are calculated. The total pressure loss coefficient  $\zeta_t$  for the main flow path is given in equation (1) and described as the total pressure difference from inlet to outlet related to dynamic head at the outlet.

$$\zeta_t = \frac{P_{t,In} - P_{t,Out}}{P_{t,Out} - P_{Out}} \quad (1)$$

Friction loss normally can be expressed as a function of diameter, pipe length and a friction factor based on empirically formulations using a local Reynolds number and wall roughness. The difficulty of this approach is that the friction loss coefficient has to be calculated for every single pipe of the junction (inlet, outlet and bleed) separately depending on the different mass flows and

cross sectional areas. After that, a global loss coefficient is determined by summing up the local loss coefficients. In respect to the STC and the geometry of the axial connection with rounded edges and hub slope this approach is unsuitable to calculate the global friction loss. But as Schlichting and Gersten (2006) state, it is possible to define the pressure loss coefficient  $\zeta_{fr}$  as a function of wall shear stress  $\tau_w$ , surface area  $A_{Sf}$  and cross sectional area  $A_{CS}$ . In equation (2)  $x$  represents the position on the meridian streamline through the corresponding pipe.

$$\zeta_{fr} = \frac{\Delta p_{fr}}{p_{t,Out} - p_{Out}} \text{ with } dp_{fr} = \frac{\tau_w(x) \cdot A_{Sf}(x)}{A_{CS}(x)} \text{ and } \Delta p_{fr} = \int \frac{\tau_w(x) \cdot A_{Sf}(x)}{A_{CS}(x)} dx \quad (2)$$

In the numerical simulation finite volumes are used why the global loss coefficient can be determined by summing up the local pressure loss for each wall element, its corresponding wall shear stress and cross sectional area (see equation (3)). At this, friction loss accuracy is directly connected to the grid density respectively the size of the wall elements.

$$\Delta p_{fr} = \sum_{i=1}^n \frac{\tau_{w,i} \cdot A_{Sf,i}}{A_{CS,i}} \quad (3)$$

Using equation (3) to replace  $\Delta p_{fr}$  in equation (2) gives the friction loss coefficient  $\zeta_{fr}$ . Subtraction the amount of friction from total pressure then leads to the secondary loss coefficient  $\zeta_{sec}$  which is comparable to the loss coefficient given by Idelchik and Miller.

$$\zeta_{sec} = \zeta_t - \zeta_{fr} \quad (4)$$

### Results for combining flow

Figure 4 shows the numerical results for combining flow in the T-junction (AR = 100 %) in comparison with measured data. As introduced in the loss description section, three different loss types are displayed in the diagram for test case C0 (water) together with deflection loss curves by Idelchik (1986) and Miller (1990). Idelchik gives only the values for pipes with sharp edge connections whereas Miller distinguishes between sharp edges (Miller case A) and rounded edges with a fillet radius of 10 % related to the hydraulic diameter (Miller case B). As illustrated in Figure 4 the numerical approach reproduces the characteristic distribution of the secondary loss coefficient  $\zeta_{sec}$  in good approximation. This indicates subtracting the amount of wall friction from total pressure loss is a suitable method to calculate secondary loss caused by deflection.

In addition to Figure 4 the distribution of secondary loss coefficient  $\zeta_{sec}$  for several area ratios is shown in Figure 5. Idelchik describes one single curve being representative for each area ratio whereas Miller specifies several curves with an area ratio AR from 50 % to 100 % (bleed area related to outlet area). Similar to Idelchik and despite various area ratios from 50 % to 100 % all curves for test case C0 are close together (Figure 5). Especially for small flow ratios and hence relevant section for the STC numerical values are in good agreement with measured data, while the losses for large flow ratios are under-predicted. Similar to the flow behaviour in a 90°-manifold, at high flow ratios due to deflection of the bleed flow a pressure gradient between inner and outer bend arises. As a result of side wall friction, cross flow perpendicular to the main flow is formed to counterbalance the pressure gradient. Interference of cross flow with main flow leads to a rise in secondary loss coefficient for pipe junctions. Pipes with circular cross sectional area like those used by Idelchik and Miller support the arising of cross flow. In contrast to this, the pipes of the T-junction don't have sidewalls by which it is not possible to form a comparable cross flow. Therefore, higher loss values depending on the additional inflow through the bleed occur for the pipe junction (Miller, Idelchik) in contrast to the rectangular and translational periodic numerical model of the T-junction without sidewalls.

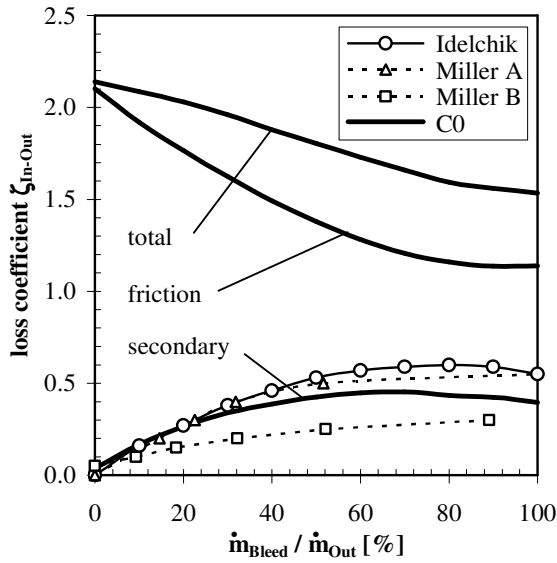


Figure 4: **Total, friction and secondary loss coefficient  $\zeta_{In-Out}$ , T-junction, test case C0, AR = 100%**

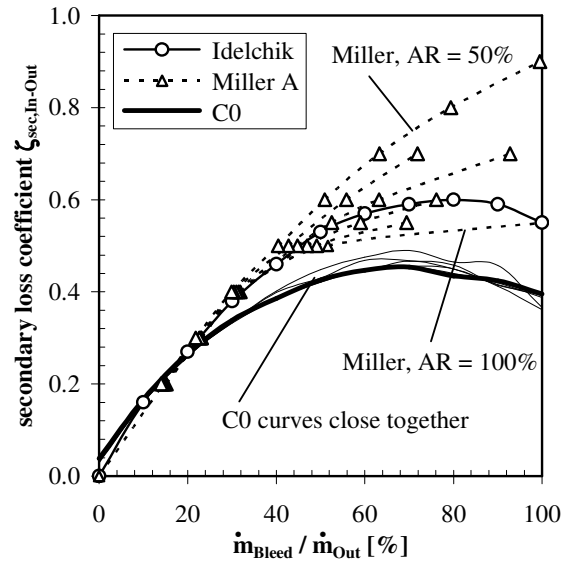


Figure 5: **Distribution of secondary loss coefficient  $\zeta_{sec,In-Out}$ , T-junction, test case C0, several area ratios**

For a zero flow ratio the numerical results do not reach a zero loss coefficient in contrast to the measurements (see Figure 5). The reason can be found in fluid partitions that enter and circulate inside the bleed channel despite full admission through the main flow path (inlet to outlet) as the left vector plot (FR = 0 %) in Figure 6 shows. When increasing the bleed mass flow two opposing effects are appearing which are illustrated with vector plots in Figure 6. On the one hand secondary losses are increased as a result of a growing separation area at the downstream edge of the T-junction (separation 2). On the other hand the losses are slightly decreased due to a reduction of the separation area at the upstream edge of the T-junction (separation 1), especially for large flow ratios (see Figure 5).

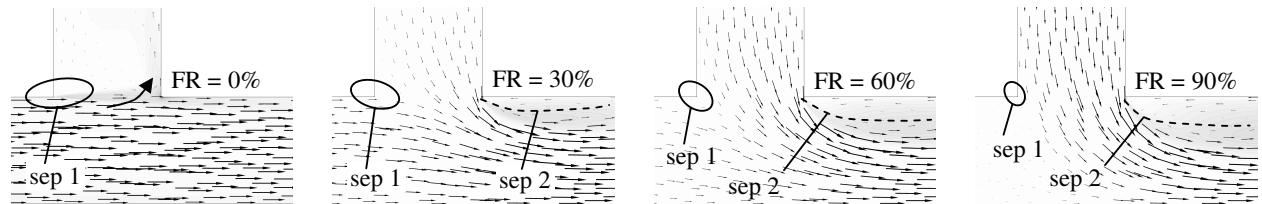


Figure 6: **T-junction vector plots for C6 with AR = 100%**

Graphs, showing results for the two numerical test case groups, fluids and turbulence models, are given in Figure 7 and Figure 8. In total all predictions show nearly similar curve characteristics. For a high amount of bleed flow the curves in Figure 7 are spread dependent on the different fluid properties of water (C0), air (C1-C3) and steam (C4, C5), whereas all used  $k-\omega$  based turbulence models in Figure 8 lead to almost the same results. Altogether, regarding the amount of friction in terms of wall shear is a viable method to gather deflection loss respectively secondary loss from total pressure loss. As Figure 7 and Figure 8 illustrate, the numerical results are in good agreement with the measurements and mostly independent from the applied fluid or turbulence model. Hence, gathered insights of the parameterised study are adaptable to the steam turbine configuration.

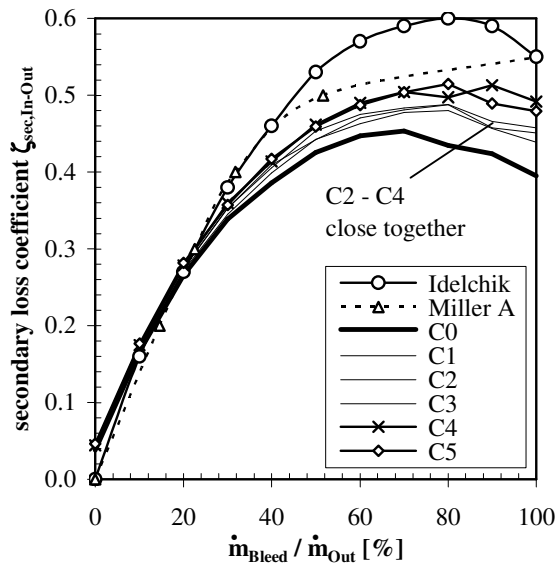


Figure 7: Distribution of secondary loss coefficient  $\zeta_{sec,In-Out}$ , T-junction, mediums C0 to C5, AR = 100%

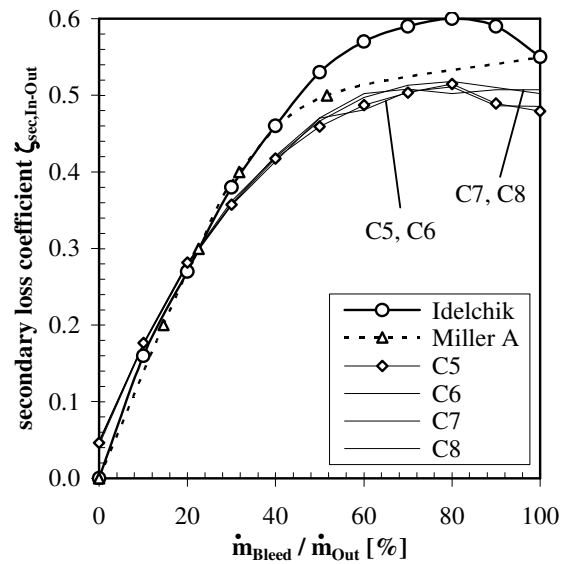


Figure 8: Distribution of secondary loss coefficient  $\zeta_{sec,In-Out}$ , T-junction, turbulence models C5 to C8, AR = 100%

### STEAM TURBINE COMPUTATIONS

Figure 9 depicts two diagrams with corresponding loss curves of the numerical results compared to the secondary loss distributions by Miller for rounded edges (equal to Miller case B in Figure 4). For similarity reasons all values are plotted against the bleed flow ratio where bleed signifies the circumferential slot in the STC case.

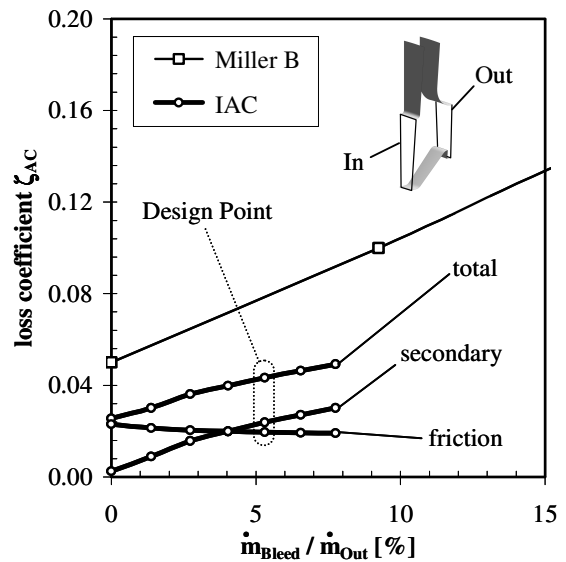
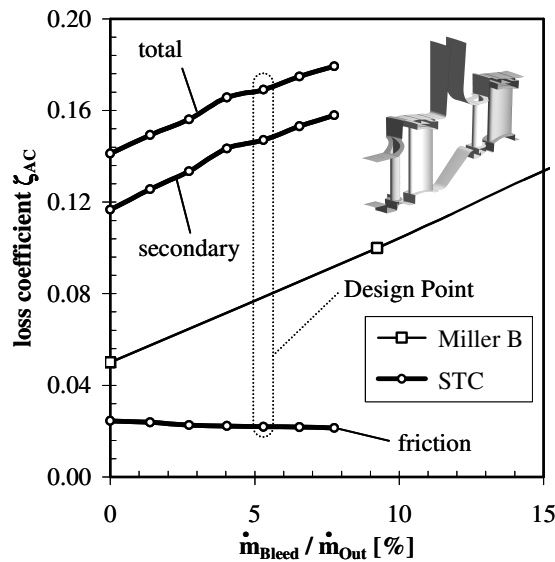


Figure 9: Total, friction and secondary loss coefficient  $\zeta_{AC}$  for steam turbine configuration with (left) and without (right) adjacent stages compared to Miller A and Miller B

In the left graph values are given for the entire STC including blades and vanes. The right graph shows results of the isolated axial connection of the STC without influence of adjacent stages (IAC). All corresponding values are gathered at the inlet and outlet of the axial connection lying between upstream rotor exit and downstream stator inlet (see Figure 9). On the one hand the amount of friction for the STC is less compared to the T-junction because of the short length of the

axial connection and concomitant minor involved wall area. On the other hand the STC contains a rounded transition at the downstream casing of the circumferential slot with a fillet ratio of 0.48 (see Table 1) whereas Miller uses a fillet ratio of 0.10 for case B. Thus, the distribution of the secondary loss coefficient  $\zeta_{\text{sec,AC}}$  for both the STC and IAC have the same slope like the results of Miller (case B) but shows a constant offset in Figure 9.

The friction loss values in Figure 9 are slightly higher for the STC than for the IAC caused by the high velocity of the shroud cavity jet leaving the upstream rotor row. However, a comparison of secondary loss for the isolated junction region of the STC to that for the STC with adjacent stages results in a  $\Delta\zeta$  of 0.11 to 0.13. As Engelmann et al. (2012) describe, this difference is attributed to the mixing of flow partitions coming from shroud cavity, main channel (rotor trailing edge) and circumferential slot in the STC. Furthermore, fluctuations arising in upstream blade rows interact with incoming slot flow while crossing the junction region. Such mixing effects and fluctuations amount to the major proportion of the secondary loss coefficient in Figure 9 (left side), are nearly constant and only slightly growing with an increase of the flow ratio. The deflection loss as a part of the secondary loss is caused by additional inflow from the circumferential slot and increases with the flow ratio for both STC and IAC. Even for the IAC, the secondary loss is higher than the friction loss above a flow ratio of 4.0 %. As the values displayed in Figure 9 show secondary losses, especially those for the design point of the STC, are too high to neglect them.

## CONCLUSIONS

In this paper an approach was presented which helps to determine deflection losses caused by additional inflow at axial stage connections. In the first part of the paper a parameterised numerical study for combining flow in a T-junction was performed using several fluids, turbulence models, flow parameters as well as various area and flow ratios. Numerical results and specific loss calculations were compared to experimental data and showed good agreement with the measurements, mostly independent from applied fluid or turbulence models. In the second part of the paper, gathered findings were adapted to the steam turbine configuration with its circumferential slot for steam admission. The results of the numerical predictions illustrate that friction loss is small compared to the other loss sources. Secondary losses caused by adjacent stages amount to the majority. Nevertheless, the deflection loss induced by additional inflow through the slot has the same order of magnitude as friction loss around the design point and is increased with the flow ratio. As a consequence, it is strongly recommended to consider the deflection loss during the design phase. The influence of the area ratio (slot related to outlet) is relatively small and therefore negligible. In contrast, the amount of deflection loss mostly depends on the flow ratio and geometric features i.e. sharp or rounded transitions as well as pipe connection or circumferential slots without sidewalls.

Future work will deal with studies for the T-junction with rounded edges as well as validation of numerical results with STC measurements. This will help to generate a new formulation in order to determine deflection loss as a function of geometry and flow ratio in 1D design tools. Further simulations with higher branch flow ratios, inflow with swirl and asymmetrical steam admission will extend the investigations and improve the physical understanding.

## ACKNOWLEDGEMENTS

The development work was conducted as a part of the joint research program COORETEC-turbo in the frame of AG Turbo. The work was supported by the Bundesministerium für Wirtschaft und Technologie (BMWi) as per resolution of the German Federal Parliament under grant number 0327787A+B. The authors gratefully acknowledge AG Turbo and MAN Diesel & Turbo SE for their support and permission to publish this paper. The responsibility for the content lies solely with its authors.

## REFERENCES

- Anker, J. E. and Mayer, J. F. (2002), Simulation of the Interaction of Labyrinth Seal Leakage Flow and Main Flow in an Axial Turbine, ASME Paper No. GT-2002-30348
- Denton, J. (1993), Loss Mechanisms in Turbomachines, ASME Paper No. 93-GT-435
- Engelmann, D., Kalkkuhl, T. J., Polklas, T. and Mailach, R. (2012), Influence of Shroud Cavity Jet and Steam Admission through a Circumferential Slot on the Flow Field in a Steam Turbine, ASME Paper No. GT2012-68465
- Giboni, A., Wolter, K., Menter, J. and Pfof, H. (2004), Experimental and Numerical Investigation into the Unsteady Interaction of Labyrinth Seal Leakage Flow and Main Flow in a 1.5 Stage Axial Turbine, ASME Paper No. GT2004-53024
- Gier, J., Stubert, B., Brouillet, B. and de Vito, L. (2003), Interaction of Shroud Leakage Flow and Main Flow in a Three-Stage LP Turbine, ASME Paper No. GT2003-38025
- Idelchik, I. E. (1986), Handbook Of Hydraulic Resistance (2nd Edition), Springer, Berlin, Diagram 7-4
- Miller, D. S. (1990), Internal Flow Systems (2nd Edition), BHRA, Figure 13.11 & Figure 13.15
- Peters, P., Breisig, V., Giboni, A., Lerner, C. and Pfof, H. (2000), The Influence of the Clearance of Shrouded Rotor Blades on the Development of the Flowfield and Losses in the Subsequent Stator, ASME Paper No. 2000-GT-478
- Pfau, A., Schlienger, J., Rusch, D., Kalfas, A. and Abhari, R. (2003), Unsteady Flow Interactions within the Inlet Cavity of a Turbine Rotor Tip Labyrinth Seal, ASME Paper No. GT2003-38271
- Schlichting, H. and Gersten, K. (2006), Grenzschicht-Theorie, 10th Edition, Springer, Berlin
- Schlienger, J. and Pfau, A., Kalfas, A. and Abhari, R. (2003), Effects of Labyrinth Seal Variation on Multistage Axial Turbine Flow, ASME Paper No. GT2003-38270
- Wagner, W., Cooper, J. R., Dittmann, A., Kijma, J., Kretschmar, H.-J., Kruse, A., Mares, R., Oguchi, K., Sato, H., Stöcker, I., Sifner, O., Takaishi, Y., Tanishita, I., Trübenbach, J. and Willkommen, T. (2000), The IAPWS Industrial Formulation 1997 for the Thermodynamic Properties of Water and Steam, ASME Journal of Turbomachinery, Vol. 122, Pages 150–182
- Wallis, A. M., Denton, J. D. and Demarge, A. A. J. (2000), The Control of Shroud Leakage Flows to Reduce Aerodynamic Losses in a Low Aspect Ratio Shrouded Axial Flow Turbine, ASME Paper No. 2000-GT-475